Identifying signatures of thermal and non-thermal reaction pathways in plasmon induced H_2 + D_2 exchange reaction

Amaraja Taur, Saurabh Kumar Singh, and Pranav R. Shirhatti*

Tata Institute of Fundamental Research Hyderabad, 36/P Gopanpally, Hyderabad 500046, Telangana, India

E-mail: pranavrs@tifrh.res.in

Phone: +91 040 20203061

Abstract

In this work we demonstrate a strategy for identifying experimental signatures of thermal and non-thermal effects in plasmon mediated heterogeneous catalytic chemistry, a topic widely debated and discussed in the literature. Our method is based on monitoring the progress of plasmon-induced (or thermally-driven) reaction, carried out in a closed system, all the way to equilibrium. Initial part of evolution of the reaction provides information about kinetics, whereas at later times the equilibrium concentrations provide information about effective temperature at the reaction sites. Combining these two pieces of information we estimate the activation energies. Using this strategy on $H_2(g) + D_2(g) \rightleftharpoons 2\,HD(g)$ isotope exchange reaction, catalyzed by Au nanoparticles under thermally-driven and light-induced conditions, we estimate the activation energies to be 0.75 ± 0.02 eV and 0.21 ± 0.02 eV, respectively. These vastly different activation energies observed are interpreted as a signature of different reaction pathways followed by the system under thermally-driven and light-induced conditions.

Introduction

Study of plasmonic nanoparticles has become an expeditiously growing field due to several exciting applications in a diverse range of fields such as chemical and biological sensing,[1–3] harvesting light energy for solar cell applications[4–6] and driving chemical reactions.[7,8] In particular, the use of plasmonic nanoparticles in the field of heterogeneous catalysis for achieving enhanced reactivity at relatively milder operating conditions has gained significant attention. The key features driving these developments are, ability to tailor properties of plasmonic nanoparticles towards harnessing light energy to catalyze chemical reactions and obtaining chemical selectivity, otherwise not readily possible using conventional methods.[9,10]

An important question emerging from these studies is regarding the nature of energy transfer from electronically excited nanoparticles to the reactants, ultimately leading to product formation. Mukherjee and coworkers[11] have reported enhanced rates of H_2 + D_2 isotope exchange reaction catalyzed by plasmonic excitation of Au nanoparticles on TiO_2 support. With the aid of first principles calculations along with experimental data, they conclude that enhanced rates result from a transient electron transfer process where the hot electrons generated from plasmonic excitation transfer to the anti-bonding orbitals of adsorbate molecules (reactants) thereby reducing the dissociation barrier. Upon using SiO_2 as a support they report up to two orders of enhancement in reaction rates, compared to TiO_2.[12] These observations were rationalized on the basis of quenching of hot carriers which is expected in case of TiO_2, but not for SiO_2. In essence, catalytic effect of plasmonic nanoparticles in this case is understood to result from generation of hot carriers (electrons) which ultimately leads to charge transfer processes and thereby driving the chemical reactions.

On the other hand, it is also well known that electronic excitation in nanoparticles can relax in a non-radiative manner by means of electron-electron and electron-phonon scattering, ultimately leading to localized heat generation.[13] This photo-thermal effect can also cause increased temperatures leading to enhanced reaction rates in a manner completely different from the hot carrier mediated pathway described above. Sivan and coworkers have argued

along these lines and have hypothesized that some of the so called plasmon-induced catalytic effects can be explained largely on the basis of localized heating of nanoparticles upon light absorption.[14,15]

Over the years, attempts have been made to understand the relative contribution of thermal and non-thermal reaction pathways and find its experimental signatures. Willets and co-workers have demonstrated this using scanning electrochemical techniques.[16,17] By a careful choice of tip and substrate potential difference for a chosen redox reaction, they are able to isolate the thermal and hot carrier mediated effects. Using surface enhanced Raman spectra of adsorbates on plasmonic nanoparticles, Linic and co-workers[18,19] have observed hyperthermal distributions of vibrational modes, which are interpreted as a signature of electron transfer like process, a key player in non-thermal catalytic pathway. A few guidelines have also been put forward recently to aid researchers in correctly interpreting and disentangling thermal vs non-thermal effects.[20–23] Despite these developments, unambiguous identification of thermal vs non-thermal effects, in general, remains a challenging task as they are often closely entangled with each other and difficult to separate due to the fast temporal and small spatial scales involved. At the same time, identifying contributions of thermal and non-thermal pathways for a given set of reaction conditions is essential to build a mechanistic understanding of plasmon-induced catalysis, a question of both fundamental and practical interest.

In this work we study the previously reported $H_2(g) + D_2(g) \rightleftharpoons 2\,HD(g)$ isotope exchange reaction, catalyzed by plasmonic Au nanoparticles supported on silica particles,[12] to understand the role of thermal vs non-thermal effects. Our method is based on following the progress of plasmon-induced reaction, carried out in a closed system, to obtain the necessary kinetic (rate constants) and thermodynamic parameters (equilibrium constant). Using equilibrium constants we estimate the effective temperatures of reaction sites under light illumination. This effective temperature combined with initial rate measurements, allows us to determine the activation energy of plasmon induced reaction. A comparison with

activation energies obtained under thermally-driven conditions (dark) allows us to identify characteristic signatures of thermal and non-thermal pathways. In the following sections we describe our experimental strategy in detail. This is followed by a description of a systematic comparison and evaluation of our results obtained under thermal (dark) and light-induced reaction conditions.

Methods

Reaction considered in this study is the isotope exchange reaction among H_2 and D_2, with gold (Au) nanoparticles supported on silica particles as a catalyst, represented by the following equation:

$$H_2(g) + D_2(g) \rightleftharpoons 2\,HD(g) \tag{1}$$

The catalyst was prepared using wet chemical deposition and precipitation method followed by heat drying, as described in the literature.[12] This resulted in formation of the catalyst in the form of a dry powder. Characterization was carried out using diffuse reflectance measurements where a strong plasmon absorption band was observed at 520 nm (see SI-1), confirming the presence of Au nanoparticles in size range of 10 to 20 nm. In a typical experiment, a loosely packed bed of catalyst was placed in the reaction chamber and purged with dry nitrogen for a few hours and subsequently, the reaction chamber was evacuated. Following this, H_2 and D_2 gases (both 99.99% pure) were filled in equal amounts with a total pressure of 1 bar. Reaction was carried out in a closed system (with intermittent sampling), either by heating the catalyst bed using a heater under dark conditions (thermal) or under light illumination of the catalyst bed (light-induced).

A schematic diagram of our experimental setup is shown in figure 1 (left panel). It consists of a custom-made stainless steel reaction chamber equipped with several gas inlets

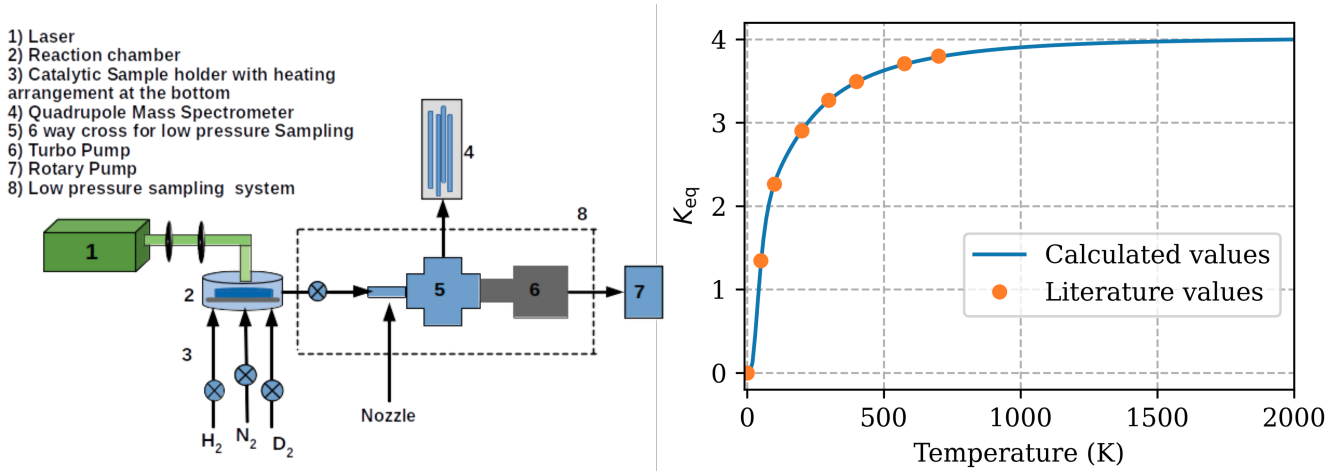

Figure 1: (left) Schematic diagram of the reaction chamber along with the mass spectrometer based detection system used to monitor the progress of the reaction. Black colored arrows with labels correspond to the inlets for reactant gases H_2, D_2 and N_2 used for purging. A small part of the gas from reactor is sent to the low pressure sampling chamber, by means of an electronically controlled solenoid valve (nozzle), for analysis using a mass spectrometer. (right) Relationship between among the temperature and K_{eq}. The markers depict data available from literature[24] and the blue line depicts the calculated values.

and a CaF_2 window to allow for illuminating the sample for plasmon-induced chemistry experiments. Progress of the reaction with time was monitored using a mass spectrometer (SRS-RGA200, quadrupole mass spectrometer) mounted on a vacuum chamber (sampling chamber), coupled to the reaction chamber via a normally closed solenoid valve (Parker 009-1643-900). The mass spectrometer was positioned away from the line of sight of the nozzle outlet. Sampling chamber was pumped by a turbo molecular pump (Hipace 80, Pfeiffer) backed by a rotary vane pump (Duo11, Pfeiffer) and had a base pressure of $1 - 5 \times 10^{-8}$ mbar (sampling off). For monitoring progress of the reaction, a small part of gas mixture (less than 1 %) from the reaction chamber was sent into sampling chamber via the solenoid valve. This valve was typically operated with a pulse duration of 100 microseconds (approx) at 30 Hz repetition rate for a duration about 60-100 sec. These settings ensured that there is a steady state build up of gas pressure in the sampling chamber (typically, $1 - 5 \times 10^{-6}$ mbar) which is detected by the mass spectrometer.

For thermal experiments, a stainless steel cup shaped holder for the catalyst bed with a

cartridge type heater attached at the bottom (outside the reaction chamber) was used. A home-built temperature controller was used to control the catalyst bed temperature within 1 K of the set temperature over the entire course of measurements. Temperature was monitored using a K-type thermocouple tip (0.3 mm diameter) immersed in the catalyst bed. Thickness of the catalyst bed was 5 mm for thermal experiments and temperature difference over this thickness was measured to be less than 3 K. Reactant gases, H_2 and D_2 were allowed to mix for 20 to 30 min in the reaction chamber before heating was started. Sampling of gas mixture was started after a steady temperature was attained on catalytic sample. For the light driven reaction, second harmonic of pulsed Nd^{+3}:YAG laser (Spectra Physics, Ascend, pulse width: 200ns, repetition rate: 1 kHz, wavelength: 532 nm) was used at different intensities. A collimated laser beam with 8 mm cross sectional diameter was made incident on the catalyst (1 mm thick bed) sample to excite the Au nanoparticles.

For both thermal and light-induced reactions, sampling performed at initial stages of the reaction was used to determine the change in fraction of HD, using which initial rate and rate constants were calculated. In the case of light-induced reaction, measurement of temperatures is particularly challenging and error prone.[14,20] Instead, we rely on a strategy where effective temperature of the reaction sites were estimated using the well-defined relationship among K_{eq} and temperature as shown in figure 1 (right panel). Here, the blue curve depicts K_{eq} evaluated using statistical thermodynamics over a range of temperatures (see SI-2 for details) and the points show values available in literature.[24] From the variation in rate constants observed with temperature, activation energies were evaluated for both light and thermally-driven reactions. A comparison of these allows us to deduce signatures of different pathways in both these cases.

In order to test the possibility of any spurious signal HD signal originating from catalytic activity of the metallic walls of the reaction chamber, control experiments were carried out with only the silica powder (Au nanoparticles absent). In case of thermally-driven reaction, HD fraction observed in absence of Au nanoparticles was smaller than 5% of the

total HD produced (SI-3). For light-induced reaction, this quantity was several orders of magnitude smaller (SI-3). These observations establish that HD production in our system is mainly catalyzed by the presence of Au nanoparticles and contribution of any other part of the reaction chamber (such as stainless steel surface etc.) is relatively much smaller. Consequently, we have ignored this small fraction of HD in further analysis of our results.

Results and discussion

Thermally-driven reaction

Progress of a typical thermally-driven reaction is shown in figure 2 (458 K, 1 bar total pressure). Top panel depicts the partial pressures measured by mass spectrometer as the reaction progresses towards equilibrium. It can be clearly seen that with increasing time H_2 and D_2 are consumed and a corresponding increase is seen in HD. Middle panel shows the fraction of H_2, D_2 and HD (f_{H_2}, f_{D_2} and f_{HD}, respectively) in the gas mixture observed as a function of time. It is worth pointing out that fractional pressures are a more robust quantity than the partial pressures themselves since variations in sampling signal caused by changes in nozzle performance over time and overall pressure increase in the reaction chamber due to temperature increase gets cancelled out. It can also be seen that at longer times (greater than 20000 seconds, approximately) the system reaches a steady state and the change in fraction (concentration) of each component is very small. Bottom panel shows the quantity $\frac{f_{HD}^2}{f_{H_2} f_{D_2}}$ plotted as a function of time. Clearly, at longer times this quantity reaches steady state, which corresponds to the equilibrium constant. It should be noted that different gases have different sensitivity factors for detection by the mass spectrometer. In these thermal experiments, since steady state temperatures of the catalyst bed (measured using a thermocouple) and hence K_{eq} are known quantities, these measurements are used to derive the gas dependent sensitivity factors. Using these gas sensitivity factors, evaluation of K_{eq} values in case of light-induced experiments (where temperature is unknown) was carried

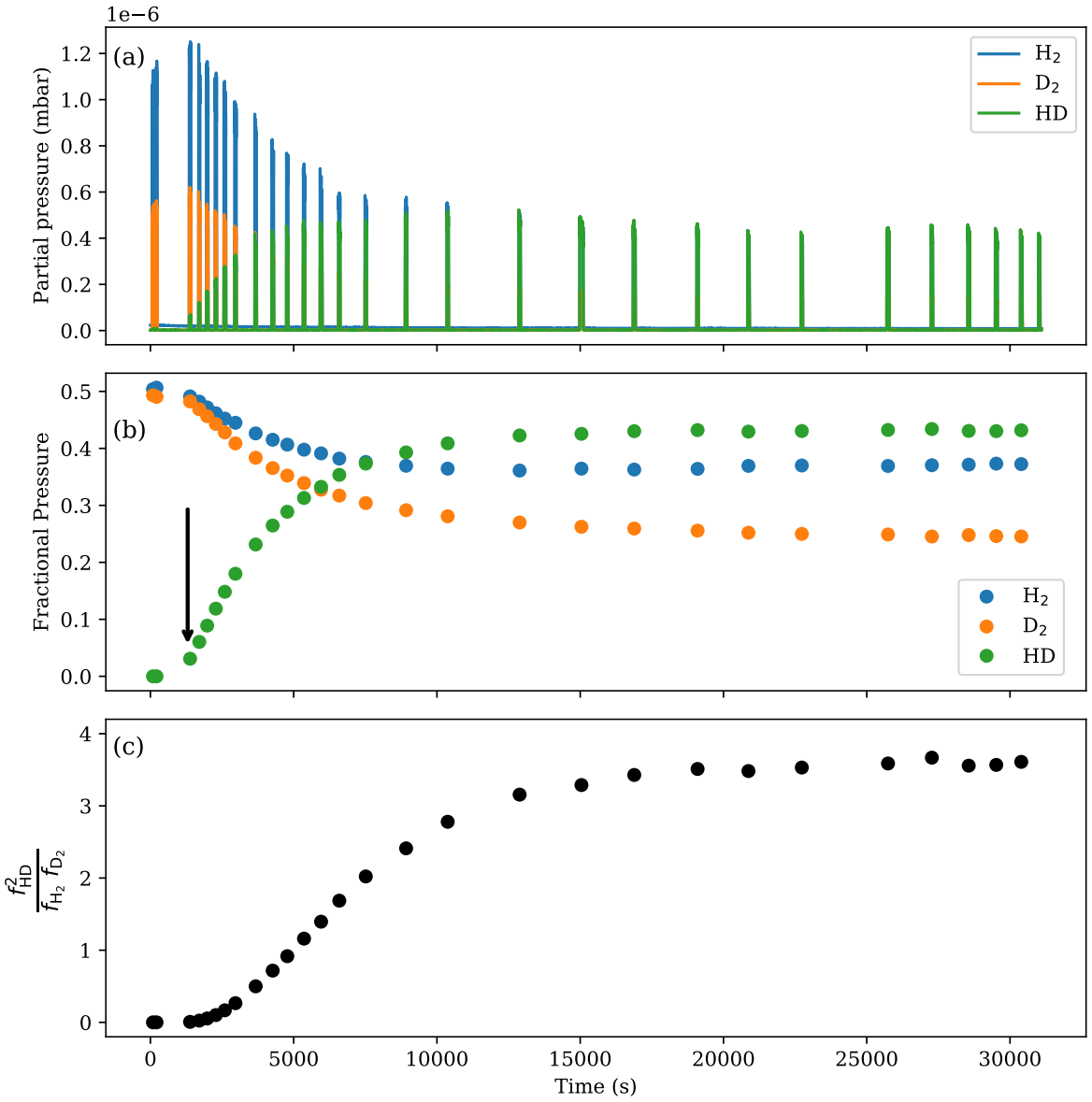

Figure 2: (a) Partial pressure of H_2, D_2, and HD measured as a function of time using mass spectrometer for thermally driven reaction (dark) with the catalyst bed at 458 K and 1 bar pressure in the reaction chamber. (b) Partial pressure fraction of the individual components (using data in panel a) plotted as a function of time. As the reaction progresses, H_2 and D_2 fractions decrease along with an increase in HD fraction, ultimately reaching a steady value at longer times. The first two measurements (around t = 0 sec) were performed before the catalyst bed was heated (at room temperature) and is used to check the initial composition of the gas mixture in the reaction chamber. The arrow corresponds to the time point where a steady temperature of 458 K was achieved. (c) $\frac{f^2_{HD}}{f_{H_2} f_{D_2}}$ as a function of time. Steady state value at longer times corresponds to the equilibrium constant under these reaction conditions.

out (see SI-4 for details).

A series of similar measurements were carried out at different temperatures ranging from (393 K to 473 K) and the quantity $\frac{\Delta f_{HD}}{f_{H_2} f_{D_2}}$ is plotted as a function of time (figure 3, left panel). This quantity denotes the change in HD fraction in the reaction chamber normalized by H_2 and D_2 fractions to account for any variations in the starting concentrations of the reaction mixture. Assuming second order kinetics for this reaction, rate of change of this quantity at given temperature, in region of initial progress of the reaction, is approximately equal to the forward rate constant (k_f) at that temperature (equation 2).

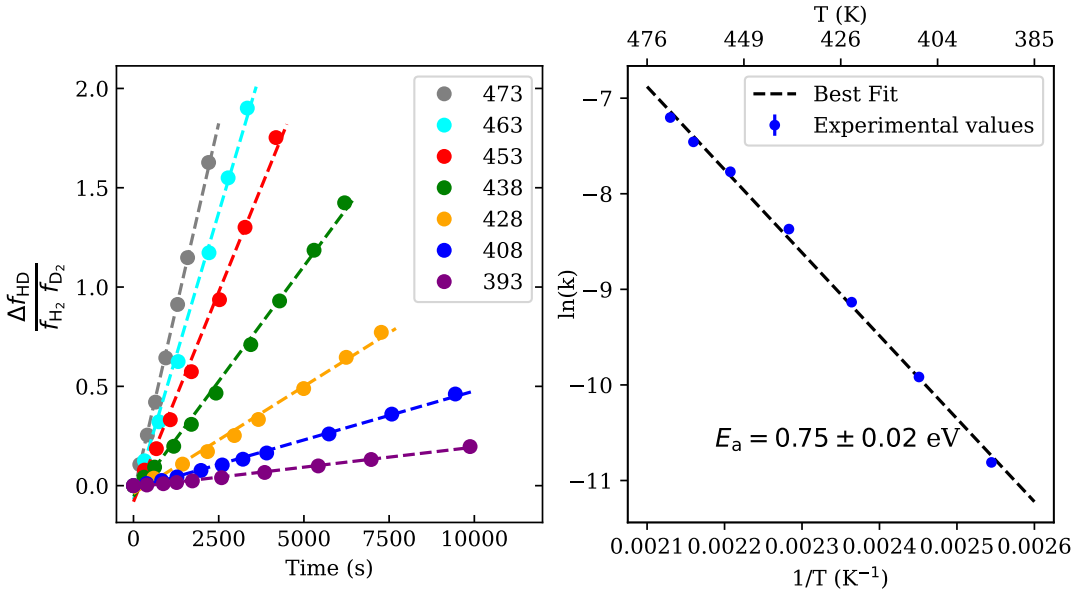

Figure 3: (left) Initial progress of the thermally driven reaction as a function of time at different steady temperatures (393 K to 473 K). The dots and dashed lines represent experimentally observed values and linear fits, respectively. (right) Arrhenius plot for determining activation energy of the thermally-driven reaction. In this case, activation energy determined from the slope of line of best fit (dashed) is 0.75 ± 0.02 eV. Uncertainty corresponds to the standard error obtained from the best fit.

$$\left[\frac{1}{p_{H_2}\ p_{D_2}} \frac{d(p_{HD})}{dt}\right]_{t=0} = k_f \tag{2}$$

It can be seen that rate of formation of HD and the corresponding rate constants (slope) increase with temperature. Logarithm of the rate constants obtained at different tempera-

tures are plotted in figure 3, right panel. Activation energy under thermally-driven conditions from this Arrhenius plot is determined to be 0.75 ± 0.02 eV.

Light-induced reaction

For the light-induced reaction, thickness of catalyst bed was reduced to 1 mm. In our experiments we observed that light absorption leads to heating of the catalyst bed, and hence a thinner sample was preferred to reduce the thermal contribution which could potentially obscure our results. Figure 4a shows progress of the reaction measured at four different average laser intensities (7.1 W/cm^2 to 11.8 W/cm^2). As observed in case of thermally-driven reaction, the quantity $\frac{f_{HD}^2}{f_{H_2} f_{D_2}}$ increases steadily with time and eventually reaches steady state yielding the equilibrium constant under these conditions. Since control experiments (in absence of Au nanoparticeles) already establish that reaction is mainly driven by the presence of Au nanoparticles, we interpret the temperature corresponding to the value of K_{eq} at a given light intensity to be a measure of energy available to the reactants at the active site. We denote this quantity as an effective temperature (T_{eff}) of the reaction site.

A closer look at these curves (figure 4b) shows that as laser intensity is increased, resulting value of K_{eq} and hence T_{eff} obtained increases systematically (see table 1). Progress of initial part of the reaction, analogous to thermally-driven case, is depicted in figure 4c. Quite clearly, as laser intensity (and hence T_{eff}) increases, rate of formation of HD and corresponding rate constants increase. Using rate constants obtained at different T_{eff}, we estimate the activation energy in this case to be 0.21 ± 0.02 eV (figure 4d). Most significant point emerging from these observations is that, activation energy obtained in the case of light-induced reaction is more than three times lower than that observed in the thermally-driven scenario (figure 4e).

Before we elaborate on the possible interpretation of these different activation energies, a careful consideration of the uncertainties and possible experimental artefacts arising from the pulsed nature of laser based illumination are discussed. Random uncertainties in our measurements arise mainly from the variations observed in partial pressure measurements.

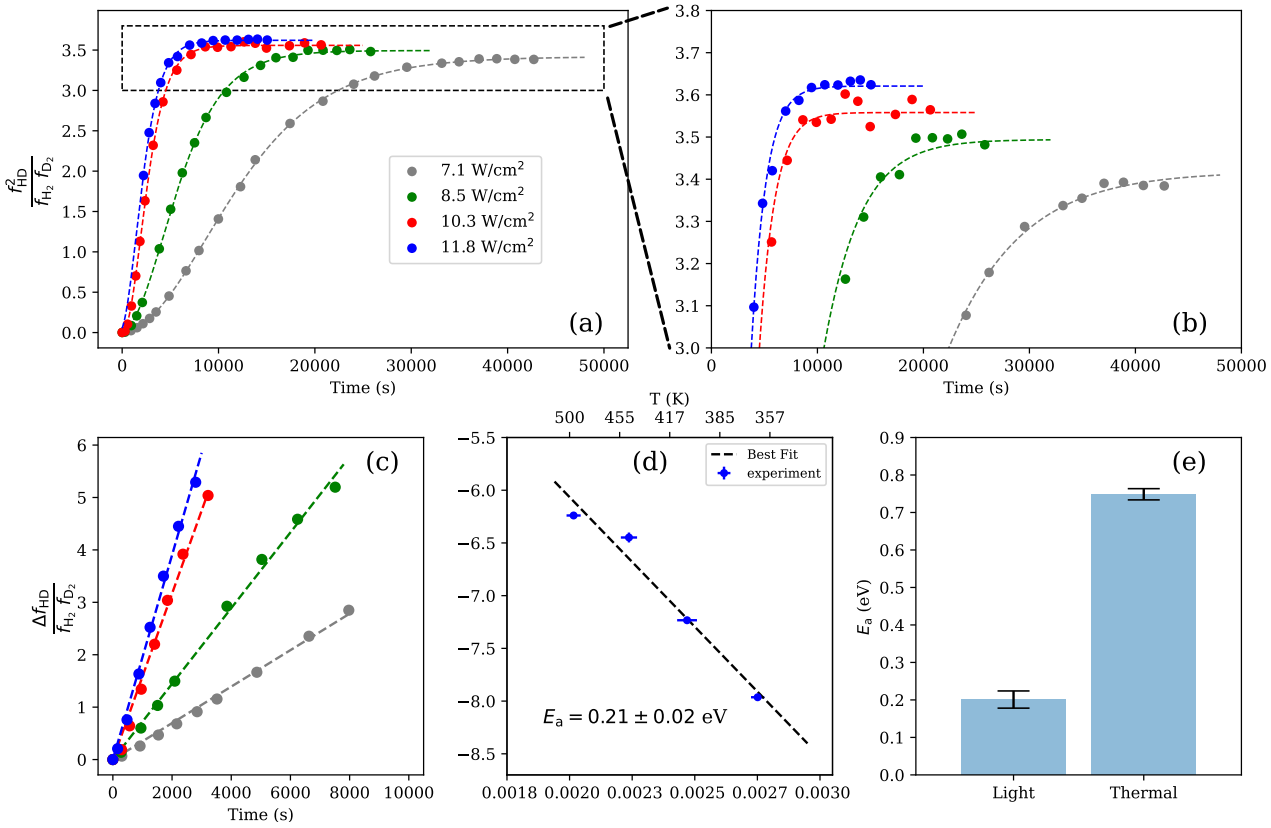

Figure 4: (a) Progress of light induced reaction as a function of time for different incident light intensity. The dashed curves show a best fit to a second order kinetics model (see SI-5). (b) A zoomed in view of the region marked by dashed rectangle in panel (a). With increasing incident light intensity, the final steady state value (equilibrium constant) and hence the T_{eff} also increases. (c) Initial progress of the light-induced reaction as a function of time at different incident intensities. (d) Arrhenius plot for determining activation energy of the light-induced reaction. For light-induced reaction, the activation energy is determined to be 0.21 ± 0.02 eV. Uncertainty corresponds to the standard error obtained from best fit. (d) Comparison of activation energies determined for the thermally-driven and light-induced reaction. Uncertainties correspond to the standard error obtained from the best fit.

Having said that, we observe that its contribution is rather small and of the order of one to two percent. Systematic errors in our measurements majorly arise from uncertainties in the determination of gas sensitivity factors, based on which the concentrations (partial pressures) of H_2, D_2 and HD are obtained. These will lead to an uncertainty in K_{eq} and hence the estimation of temperatures. However, even a conservative estimate of $\pm 5\%$ uncertainty in the calibration factors does not make much difference to the calculated activation energies. Most importantly, qualitative nature of these results remain same i.e., activation energy in case of light-induced reaction is much lower than its thermal counterpart.

Another point that needs to be considered is that the pulsed laser used in our measurements can possibly cause a much larger temperature jump due to transient heating, leading to an underestimation of T_{eff} and hence the activation energy. In order to understand if this problem affects our measurements or not, a separate series of measurements under similar experimental conditions were carried out, to compare the results obtained using a pulsed vs c/w illumination (Sprout-D5W, Lighthouse Photonics, 532 nm). Progress of the reaction observed with pulsed vs c/w laser illumination is shown in figure 5. These results show quite clearly that initial rates observed for c/w and pulsed laser experiments, carried out under similar experimental conditions are very close to each other. Although this comparison is limited to relatively lower intensities that are available from our c/w laser, the close correspondence among the observed rates suggests that this trend should also hold true at higher intensities too. Based on these observations, we believe that any major differences resulting from the pulsed vs c/w nature of light used in our experiments can be ruled out. Consequently, any underestimation of T_{eff} in case of pulsed laser based experiments can also be ruled out.

Above presented results clearly show that activation energy for light-induced reaction is much lower than the thermally-driven case. We interpret this large difference in activation energies as a signature of different reaction pathways followed under thermally driven and light induced conditions. These observations are also qualitatively consistent with the earlier

proposed hypothesis based on first principles calculations,[11] where it was suggested that plasmonic excitation causes transient electron transfer to the adsorbate molecules leading to bond weakening, thereby lowering the activation barrier and leading to enhanced reaction rates compared to the thermal reaction pathway.

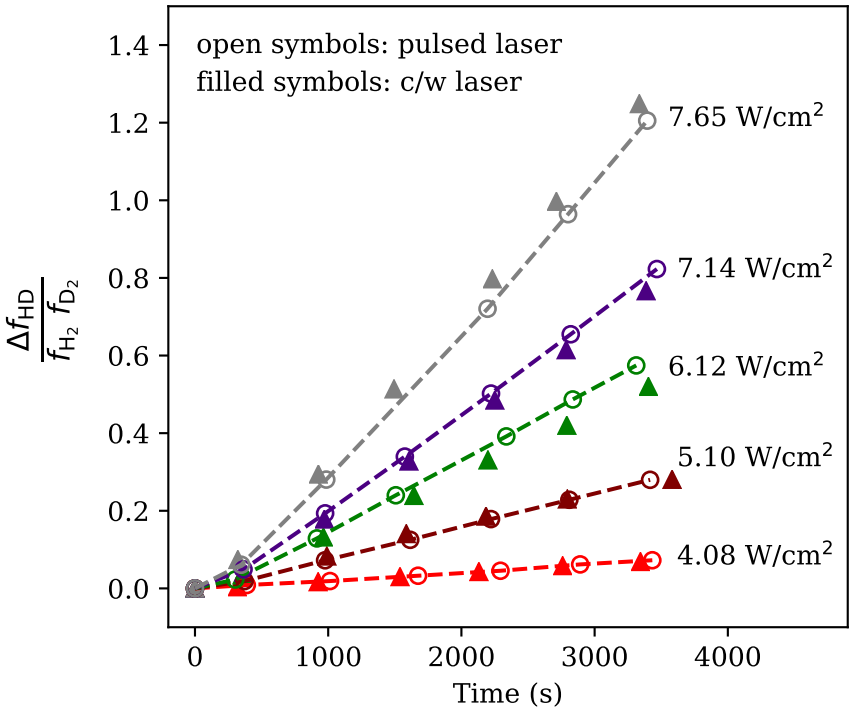

Figure 5: Comparing initial progress of the light-induced reaction under illumination with pulsed (open circle) and c/w laser (filled triangles) for different incident intensities (other reaction conditions kept same). Dashed lines depict linear fit to the data points obtained with pulsed laser, and have been included to indicate the trend. For a given incident intensity, the observed initial rates using pulsed or c/w laser are very similar. This rules out any major artefacts in T_{eff} estimation based on the equilibrium measurements done with the pulsed laser (see results and discussion for details).

Another point worth highlighting here is that, the activation energy for the thermally driven reaction is estimated to be 0.75 ± 0.02 eV, which is significantly lower than the ground state barrier of 2.3 eV estimated from first principle simulations.[11] At this moment based on these results alone, it is not possible for us to pinpoint the exact reason behind this discrepancy. Nonetheless, we believe that our experimentally determined values will provide a valuable reference for comparison with theoretical estimates in future.

Table 1: Equilibrium constant and respective effective temperatures obtained at different laser intensities for the light-induced reaction. Uncertainties denote standard error obtained from fitting .

Intensity (W/cm^2)	K_{eq}	T_{eff} (K)
7.1	3.418±0.007	363.5±4
8.5	3.494±0.011	405±7
10.3	3.559±0.009	447±7
11.8	3.621±0.008	496±7

Concluding Remarks

This work demonstrates a robust experimental strategy by means of which we identify distinct signatures of thermal and non-thermal pathways in plasmon induced H_2 + D_2 exchange reaction. Much lower activation energies obtained in case of light-induced compared to the thermal reaction is indicative different pathways followed by the system under these conditions. These observations are consistent with the idea that for the reaction under study, plasmon-driven reactions are assisted by the hot carriers which leads to an reduced activation barrier, a pathway which is different from the thermally driven reaction under dark conditions. Finally, we believe that the measurement strategy presented in this work based on determining kinetic and thermodynamic parameters using a closed system is robust and widely applicable as it can be extended to different plasmon-driven chemical reactions. This will greatly contribute to our understanding of thermal vs non-thermal effects and mechanistic aspects of plasmon-induced chemistry in general.

Acknowledgement

This work was supported by intramural funds at TIFR Hyderabad from the Department of Atomic Energy, Government of India. The authors acknowledge our institute mechanical workshop staff Rakesh Mudike and Brahma for fabricating the reaction chamber and several components used in our experimental setup. We thank M. Krishnamurthy, Ram Gopal and Gaurav Rajput for access and help with the laser systems, T.N. Narayanan for access to wet

lab facilities for catalyst preparation, Shourya Dutta Gupta and Jayakumar (Indian Institute of Technology - Hyderabad) for their help in diffuse reflection measurements and Geetika Bhardwaj for building the temperature controller.

Supporting Information Available

- SI-1: Diffused reflectance spectrum of Au nanoparticles supported on silica
- SI-2: Estimating temperatures from equilibrium constant measurements
- SI-3: Background HD contribution to the reaction
- SI-4: Estimating gas dependent sensitivity factors for our detection setup
- SI-5: Second order kinetics model used for fitting

Author Contributions

AT designed, tested the experimental setup and carried out the measurements with contributions from SKS and PRS. AT and SKS analyzed the results with inputs from PRS. PRS conceived the project and provided conceptual inputs. AT and PRS prepared the manuscript with inputs from SKS. All authors discussed the results and the manuscript.

References

(1) Larsson, E. M.; Langhammer, C.; Zorić, I.; Kasemo, B. Nanoplasmonic Probes of Catalytic Reactions. *Science* **2009**, *326*, 1091–1094.

(2) Tittl, A.; Giessen, H.; Liu, N. Plasmonic gas and chemical sensing. *Nanophotonics* **2014**, *3*, 157–180.

(3) Willets, K. A.; Van Duyne, R. P. Localized Surface Plasmon Resonance Spectroscopy and Sensing. *Annual Review of Physical Chemistry* **2007**, *58*, 267–297.

(4) Atwater, H. A.; Polman, A. Plasmonics for improved photovoltaic devices. *Nature Materials* **2010**, *9*, 205–213.

(5) Catchpole, K. R.; Polman, A. Plasmonic solar cells. *Optics Express* **2008**, *16*, 21793.

(6) Pillai, S.; Catchpole, K. R.; Trupke, T.; Green, M. A. Surface plasmon enhanced silicon solar cells. *Journal of Applied Physics* **2007**, *101*, 093105.

(7) Brongersma, M. L.; Halas, N. J.; Nordlander, P. Plasmon-induced hot carrier science and technology. *Nature Nanotechnology* **2015**, *10*, 25, Publisher: Nature Publishing Group, a division of Macmillan Publishers Limited. All Rights Reserved.

(8) Linic, S.; Aslam, U.; Boerigter, C.; Morabito, M. Photochemical transformations on plasmonic metal nanoparticles. *Nature Materials* **2015**, *14*, 567–576.

(9) Robatjazi, H.; Zhao, H.; Swearer, D. F.; Hogan, N. J.; Zhou, L.; Alabastri, A.; McClain, M. J.; Nordlander, P.; Halas, N. J. Plasmon-induced selective carbon dioxide conversion on earth-abundant aluminum-cuprous oxide antenna-reactor nanoparticles. *Nature Communications* **2017**, *8*, 27.

(10) Marimuthu, A.; Zhang, J.; Linic, S. Tuning Selectivity in Propylene Epoxidation by Plasmon Mediated Photo-Switching of Cu Oxidation State. *Science* **2013**, *339*, 1590–1593, Publisher: American Association for the Advancement of Science.

(11) Mukherjee, S.; Libisch, F.; Large, N.; Neumann, O.; Brown, L. V.; Cheng, J.; Lassiter, J. B.; Carter, E. A.; Nordlander, P.; Halas, N. J. Hot Electrons Do the Impossible: Plasmon-Induced Dissociation of H_2 on Au. *Nano Lett.* **2013**, *13*, 240.

(12) Mukherjee, S.; Zhou, L.; Goodman, A. M.; Large, N.; Ayala-Orozco, C.; Zhang, Y.; Nordlander, P.; Halas, N. J. Hot-Electron-Induced Dissociation of H_2 on Gold Nanoparticles Supported on SiO)2. *Journal of the American Chemical Society* **2014**, *136*, 64–67.

(13) Amendola, V.; Pilot, R.; Frasconi, M.; Maragò, O. M.; Iatì, M. A. Surface plasmon resonance in gold nanoparticles: a review. *Journal of Physics: Condensed Matter* **2017**, *29*, 203002.

(14) Sivan, Y.; Baraban, J.; Un, I. W.; Dubi, Y. Comment on "Quantifying hot carrier and thermal contributions in plasmonic photocatalysis". *Science* **2019**, *364*, eaaw9367.

(15) Sivan, Y.; Un, I. W.; Dubi, Y. Assistance of metal nanoparticles in photocatalysis – nothing more than a classical heat source. *Faraday Discussions* **2019**, *214*, 215–233.

(16) Yu, Y.; Williams, J. D.; Willets, K. A. Quantifying photothermal heating at plasmonic nanoparticles by scanning electrochemical microscopy. *Faraday Discussions* **2018**, *210*, 29–39.

(17) Yu, Y.; Sundaresan, V.; Willets, K. A. Hot Carriers versus Thermal Effects: Resolving the Enhancement Mechanisms for Plasmon-Mediated Photoelectrochemical Reactions. *The Journal of Physical Chemistry C* **2018**, *122*, 5040–5048.

(18) Boerigter, C.; Aslam, U.; Linic, S. Mechanism of Charge Transfer from Plasmonic Nanostructures to Chemically Attached Materials. *ACS Nano* **2016**, *10*, 6108–6115.

(19) Boerigter, C.; Campana, R.; Morabito, M.; Linic, S. Evidence and implications of direct charge excitation as the dominant mechanism in plasmon-mediated photocatalysis. *Nature Communications* **2016**, *7*.

(20) Zhang, X.; Li, X.; Reish, M. E.; Zhang, D.; Su, N. Q.; Gutiérrez, Y.; Moreno, F.; Yang, W.; Everitt, H. O.; Liu, J. Plasmon-Enhanced Catalysis: Distinguishing Thermal and Nonthermal Effects. *Nano Letters* **2018**, *18*, 1714–1723.

(21) Sivan, Y.; Baraban, J. H.; Dubi, Y. Experimental practices required to isolate thermal effects in plasmonic photo-catalysis: lessons from recent experiments. *OSA Continuum* **2020**, *3*, 483.

(22) Baffou, G.; Bordacchini, I.; Baldi, A.; Quidant, R. Simple experimental procedures to distinguish photothermal from hot-carrier processes in plasmonics. *Light: Science & Applications* **2020**, *9*.

(23) Jain, P. K. Taking the Heat Off of Plasmonic Chemistry. *The Journal of Physical Chemistry C* **2019**, *123*, 24347–24351.

(24) Urey, H. C.; Rittenberg, D. Some Thermodynamic Properties of the H ^{1} H ^{2} , H ^{2} H ^{2} Molecules and Compounds Containing the H ^{2} Atom. *The Journal of Chemical Physics* **1933**, *1*, 137–143.